Princeton/$\mu\mu$/98-11
S.E. Vahsen and K.T. McDonald
July 25, 1998

Precision Timing via Čerenkov Radiation

Abstract

A simulation indicates that the rms timing, σ_t, of 165-MeV/c muons could be determined over a beam of 10-cm radius to 10 ps via Čerenkov radiation emitted in 1×1 cm^2 quartz bars viewed by Hamamatsu R3809U microchannel-plate photomultipliers. The simulation is validated by comparison with recent measurements with 1.5-GeV/c pions. This technique would provide an excellent secondary timing measurement for the proposed muon-cooling demonstration experiment, and nearly meets the requirements for the primary timing measurement.

1 Introduction

We have simulated the timing signal obtained when charged particles traverse a quartz bar, emitting Čerenkov radiation which is detected by photomultipliers.

This work was motivated by the need for a timing measurement in the proposed muon cooling experiment [1], in which all 6 phase-space parameters of individual, unbunched muons are to be measured before and after cooling. Then any desired input bunch in muon phase space can be formed in software and the effect of the cooling apparatus can be calculated for the corresponding output bunch.

The most demanding measurement is that of the time t of individual muons relative to the phase of the 805-MHz rf in the linacs of the cooling apparatus. The time must be known to 8 ps at the entrance and exit of the cooling channel. In the baseline scenario (Fig. 1) [2], this is accomplished via rf-timing cavities which change the momentum of a muon by an amount proportional to time offset between the muon and the null point of the field. By measuring the momentum before and after the rf-cavity, the time offset can be obtained with an estimated accuracy of $\sigma_t = 6$ ps. The extrapolation of this result from the position of the rf cavity to the cooling channel increases the uncertainty to 8 ps.

However, this measurement of a time t is ambiguous with time $T/2 - t$, where T is the rf period. Thus, we need an additional timing measurement with $\sigma_t \lesssim T/8 \approx 150$ ps to resolve the ambiguity.

The second measurement together with that from the rf-timing cavity could serve to distinguish muons from electrons and pions by time of flight, if the accuracy of the second measurement satisfies $\sigma_t < 50$ ps [2]. Finally, if the second timing measurement has an accuracy $\sigma_t \leq 6$ ps, there might be no need for the rather costly rf-timing apparatus.

Kichimi *et al.* [3] recently reported rms time resolution, σ_t, better than 25 ps for the detection of 1.5-GeV/c pions, using Hamamatsu H2431 fine-mesh PMT's to view Čerenkov

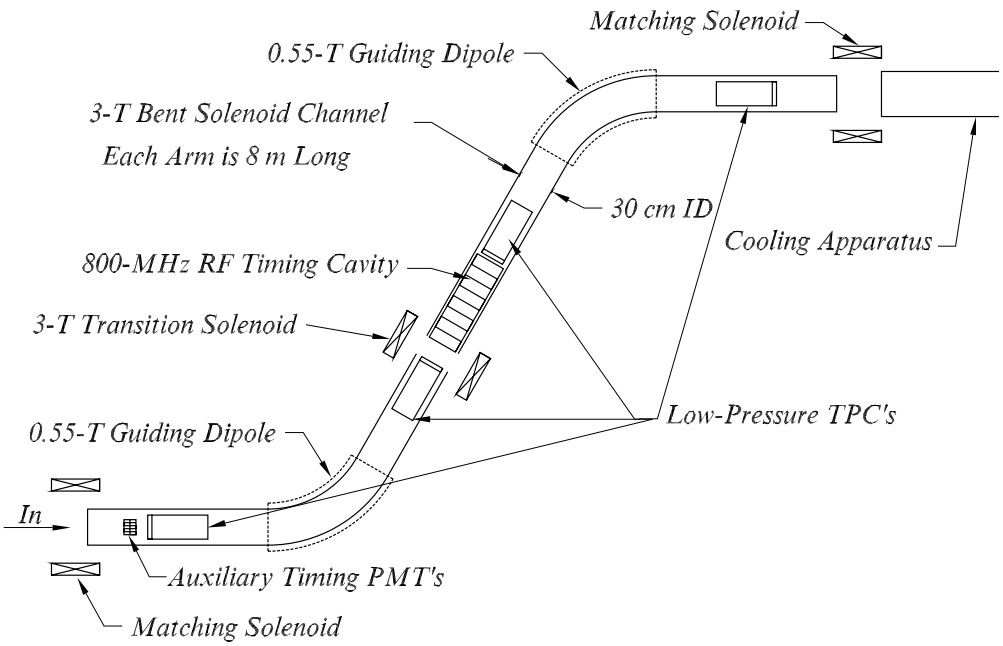

Figure 1: Sketch of the detectors used to measure all 6 phase-space coordinates of a muon before it enters the proposed cooling apparatus [1].

light from quartz bars. This is less than one fifth of the nominal transit-time spread, $\sigma_{\rm TT} = 160$ ps, quoted for those PMT's. Encouraged by this result, we desired to predict the time resolution that could be obtained with faster PMT's. For instance, Hamamatsu reports the transit-time spread of their microchannel-plate photomultiplier (MCP-PMT) R3809U to be as low as $\sigma_{\rm TT} = 11$ ps [4].

2 Simulated Scenario

Our simulation estimates the timing characteristics of Čerenkov photons due to a high-energy particle passing through a quartz bar. Some of the photons will travel to the end of the bar by total internal reflection (TIR), where they are detected with a specified efficiency by photomultipliers. From analysis of the timing statistics of the observed photons for various bar geometries and track angles, we can estimate the timing capabilities of such configurations and optimize the detector parameters.

A run of the simulation consists of a given number of events, typically 500-5000, in each of which the Čerenkov radiation from a single particle is analyzed. In a particular run of the simulation, the particles all have the same energy and angle of incidence θ_i (0° is normal incidence) on a bar of thickness d, and all enter the bar at time $t = 0$ at the same point at distance z from the face of the photomultiplier along the axis of the bar.

The simulation is based on a Microsoft EXCEL worksheet that we obtained from Mats Selen. Even though a single worksheet generally does not allow the iterative procedures

needed for a run of multiple events, we implemented these by writing scripts in Visual Basic (VBA) that pass data between segments of a worksheet. Multiple runs, in which one or more of the particles' initial parameters are varied, were also processed iteratively in a single EXCEL worksheet.

The number of Čerenkov photons radiated by the test particle in the quartz bar is calculated according to

$$N = \frac{d}{\cos\theta_i}\frac{2\pi\alpha}{c}\int \sin^2\theta_C \; d\nu = \frac{d}{\cos\theta_i} 2\pi\alpha \int \sin^2\theta_C \; \frac{d\lambda}{\lambda^2}, \tag{1}$$

where the Čerenkov-cone half angle is given by

$$\theta_C(\lambda) = \cos^{-1}\frac{1}{\beta n(\lambda)}, \tag{2}$$

$n(\lambda)$ is the wavelength-dependent index of refraction (dispersion), $\beta = v/c$ is the velocity of the particle, $\alpha \approx 1/137$ is the fine-structure constant, and $d\nu$ ($d\lambda$) is the frequency (wavelength) interval over which the photons are detected. For example, $n \approx 1.47$ in quartz so $\theta_C \approx 45^\circ$ and $N \approx 500/\text{cm}$ for the wavelength interval $300 < \lambda < 600$ nm. This number is large enough that we ignore fluctuations in it.

A single event of the simulation proceeds as follows. N Čerenkov photons are generated uniformly at random along the particle track within the quartz bar. The simulation does not include δ-rays, which are reported to contribute about one Čerenkov photon per cm of particle track in quartz [3]. Each photon is assigned a frequency which is uniformly distributed at random over a specified interval. The distances z' between the point of emission of the photon and the photomultiplier and d' between the point of entrance of the particle and the point of emission of the photon are also calculated.

The photons are emitted in a cone with halfangle $\theta_C(\lambda)$ to the particle track, uniformly distributed at random in azimuthal angle. The photons are not tracked down the quartz bar in detail. Rather, the initial direction cosines of each photon relative to the bar axes are used to calculate whether the photon will be internally reflected at the faces of the quartz bar, and those photons that are not reflected are disregarded. Photons not propagating towards the photomultiplier are disregarded. The quartz bar is coupled to the photomultiplier through a thin layer of material of index $n' = 1.40$; a photon is disregarded if its direction is such as to be internally reflected at this interface. The attenuation of light in the quartz is characterized by a wavelength-dependent attenuation length $\Lambda(\lambda)$, and a photon is disregarded by a random selection with probability $1 - \exp(-l/\Lambda)$, where $l = z'/\cos\theta_z$ is the actual pathlength of the photon with direction cosine $\cos\theta_z$ in the quartz bar. The attenuation curve used in the simulation is based on the transmittance of UV-grade quartz given in Fig. 2(top).

The response of the photomultiplier to photons which strike the photocathode is described by wavelength dependence of the quantum efficiency $\text{QE}(\lambda)$, as shown in Fig. 3. A photon is disregarded by a random selection with probability $1 - \text{QE}(\lambda)$.

Čerenkov photons passing the above cuts are considered to be detected, and the time of detection is calculated as $ct = d'/\beta + z'/[n(\lambda)\cos\theta_z]$. The transit-time jitter of the PMT is simulated by adding a Gaussian-distributed random time offset with standard deviation σ_{TT} to time t.

No simulation is made of the PMT output pulse shape.

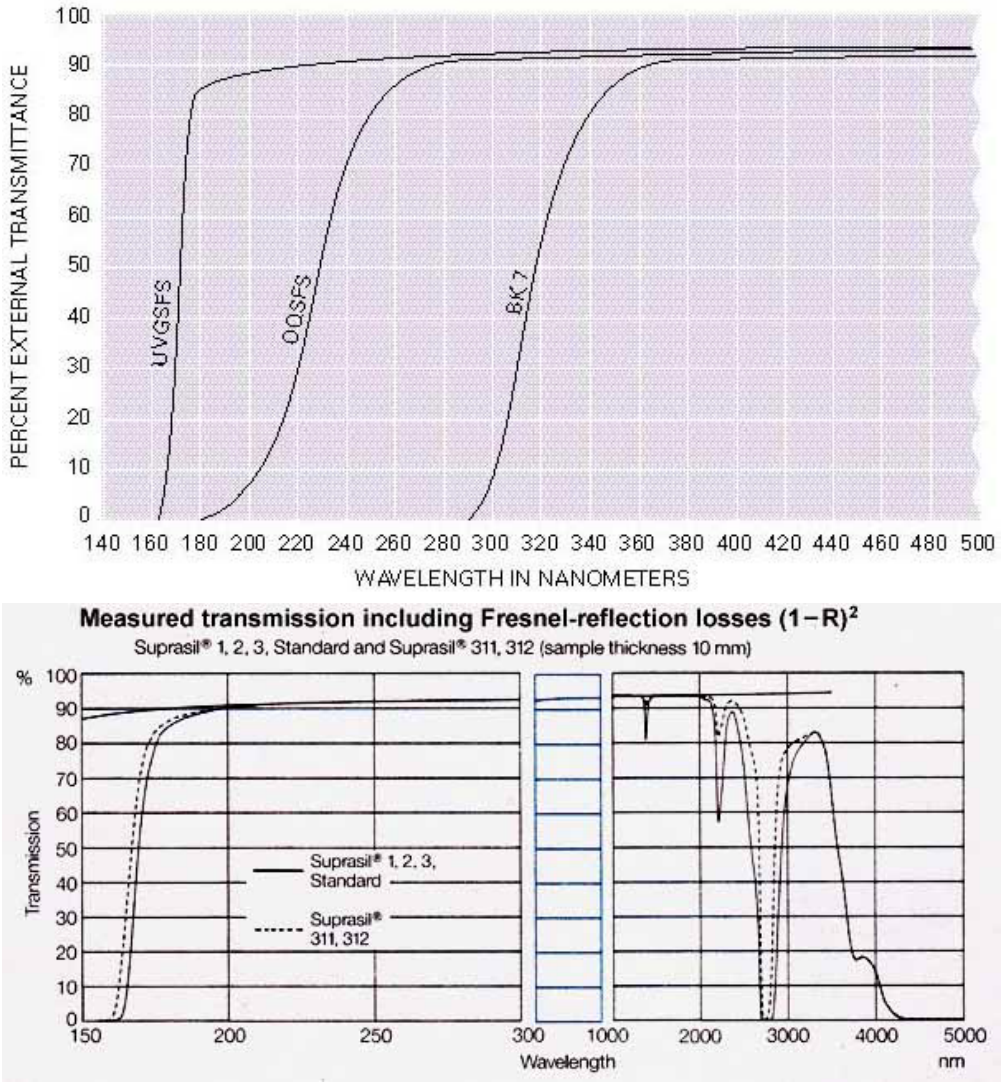

Figure 2: The transmittance of UV-grade quartz *vs.* wavelength for 1-cm-thick samples, including the 8% reflection losses at the surfaces. Top: As reported in the Melles-Griot catalog [5], which results were used in the present study. Bottom: Suprasil fused silica from Hereaus [6], which can have somewhat better transmittance than that reported by Melles Griot.

3 Photon Yield

As a first verification of our simulation, we compare the predicted number of photons detected for a 1.5-GeV/c π^- beam incident on a $2 \times 4 \times 120$ cm^3 quartz bar with the results of Kichimi *et al.* [3]. See Fig. 4.

The number of photons observed depends strongly on the pion's angle of incidence θ_i, which changes the pion's track length, as well as the conditions for internal reflection. The 1.5-GeV/c pions give rise to Čerenkov light at an angle $\theta_C = 47^\circ$ to the pion's track. The

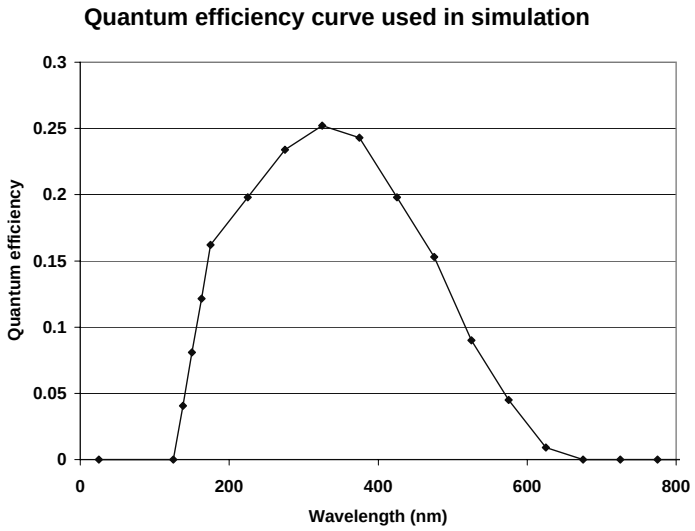

Figure 3: The wavelength dependence of the quantum efficiency used in the simulation. The gentle dropoff at wavelengths below 400 nm occurs because the semitransparent photocathode is too thin for full absorption of short-wavelength photons [7]. The steep dropoff at wavelengths below 175 nm is due to absorption in the glass face of the PMT.

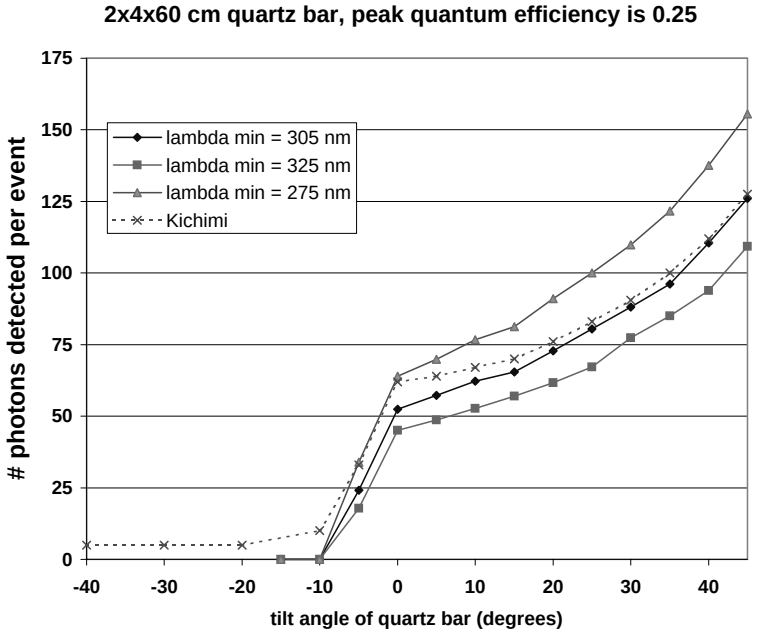

Figure 4: Observed [3] and predicted Čerenkov-photon yield for 1.5-GeV/c pions incident on a $2 \times 4 \times 120$ cm^3 quartz bar. The number of observed photons has a strong dependence on the angle of incidence, θ_i, as well as on the short-wavelength cutoff $\lambda_{\rm min}$.

critical angle for TIR at the quartz($n = 1.47$)/air boundary is 43°. We therefore don't expect to observe Čerenkov photons for $\theta_i < -7°$. (Some photons with nonzero azimuthal angle can be captured by TIR when $-7° < \theta_i < -4°$.) The photons observed with $\theta_i < -7°$ are due to δ-rays, and their timing-characteristics are not obvious. Yet, their effect on the overall time resolution could only be an improvement, since they increase the overall amount of time information per event. Since our simulation does not include δ-rays, we should obtain conservative estimates of the time resolution.

In the experiment by Kichimi *et al.*, the main limitation on bandwidth in the low wavelength range was the transparency of the borosilicate window on the photocathode (whose effective detection range is 300 to 600 nm). In the simulation corresponding to that experiment, we therefore impose a cut that excludes photons with wavelength shorter than $\lambda_{\min}$. Since the photons are uniformly distributed in energy (or frequency), there are more photons in the short-wavelength range, and the photon yield is therefore very sensitive to the short wavelength cutoff $\lambda_{\min}$. By setting $\lambda_{\min} = 305$ nm we obtain a good fit to the experimental data after subtracting the contribution of about five photons/event from δ-rays.

4 Time Resolution

The comparison of predicted time resolution against experiment provides another test of our simulation. For the conditions used in the experiment of Kichimi *et al.*, our simulation predicts the Čherenkov photons to arrive in pulses characterized by a FWHM ranging from 9 ps (5-cm bar, $\theta_i = 40°$, Fig. 5(top)) to 110 ps (115-cm bar, $\theta_i = 0°$, Fig. 5(bottom)).

Kichimi *et al.* obtained their timing signal by feeding the PMT output into a discriminator "set at 50 mV, which corresponded to a few photoelectron signal" [3]. In our simulation, we do not take the PMT output pulse shape into account. Since the predicted pulse width of the arriving photons is short compared to the 0.7-ns rise time of the Hamamatsu H2431 PMT used in the experiment, we make the approximation that the PMT output that triggered the discriminator corresponds to a fixed number of photons having arrived.

The uncertainty in the timing of a charged particle is therefore simulated as the uncertainty in the arrival time of the *nth* arriving photon, where the number n remains to be determined. For each event in the simulation, the arrival-times (smeared by the PMT transit-time jitter) of all Čerenkov photons that satisfy the detector cuts are sorted in order of increasing time and stored. After the run has been completed, we calculate the standard deviation $\sigma_{t,n}$ of the distribution of the nth arriving photon. Figure 6 shows the results with and without PMT transit-time jitter for two different configurations, corresponding to the best and worst timing cases in the experiment of Kichimi *et al.*

Even though the first photon generally has the least time jitter when it arrives at the face of the PMT, the effect of the PMT transit-time jitter is such that one can obtain better timing based on the arrival time of a later photon. This occurs whenever the transit-time jitter $\sigma_{\rm TT}$ of the PMT is large compared to the intrinsic time jitter $\sigma_{t,1}$ of the earliest arriving photon (not including the smearing by $\sigma_{\rm TT}$).

It appears that Kichimi *et al.* used the same discriminator threshold for all distances z between PMT and particle track and all angles of incidence. Hence we must choose a single value of photon-arrival number n in our simulation of all z and θ_i. We achieve a

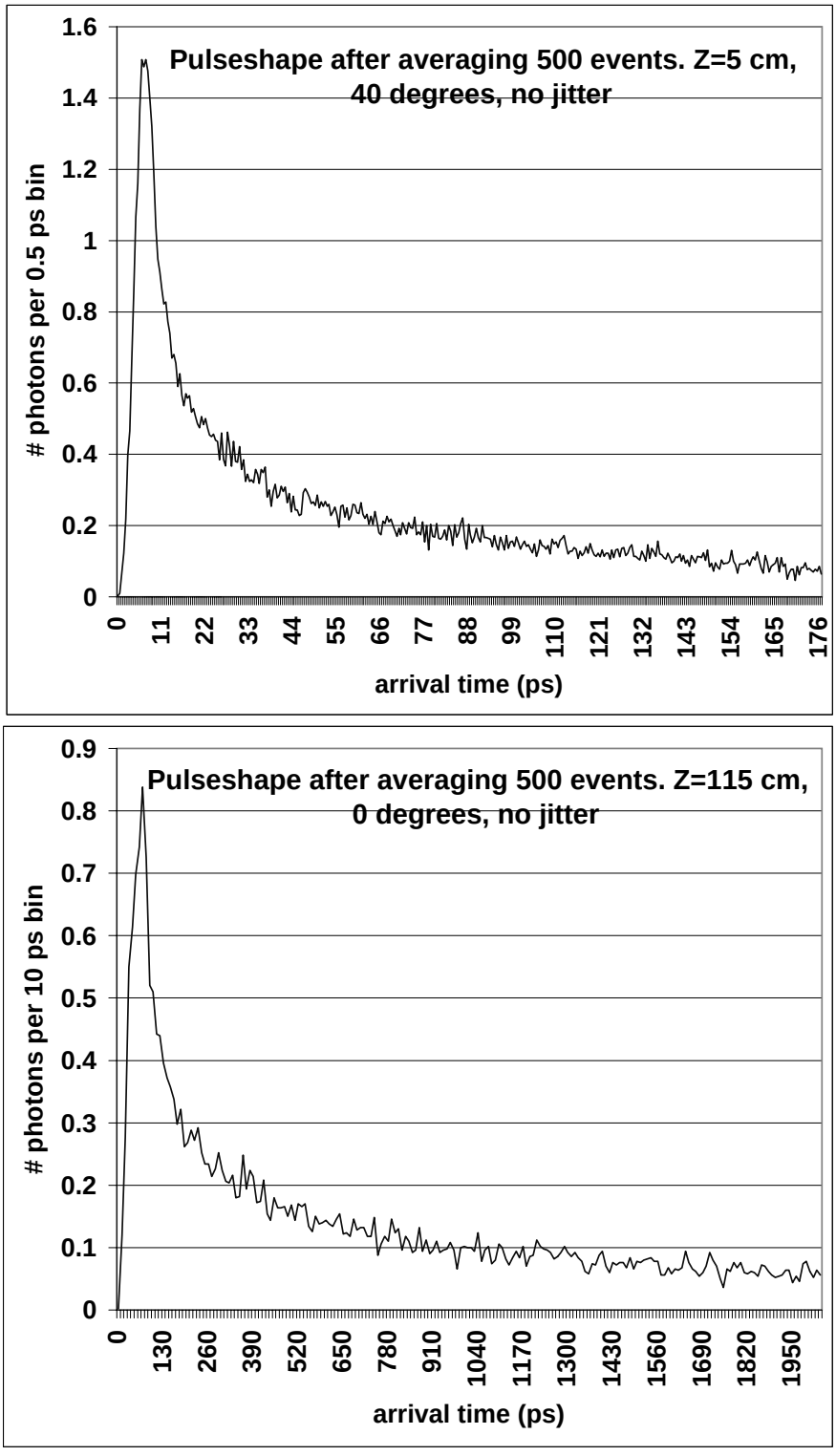

Figure 5: Simulated distributions of arrival times at the face of the PMT of Čerenkov photons in 2×4 cm^2 quartz bars for 1.5-GeV/c pions incident at 5 cm (top) and 115 cm (bottom) from the PMT. Transit-time jitter is not included.

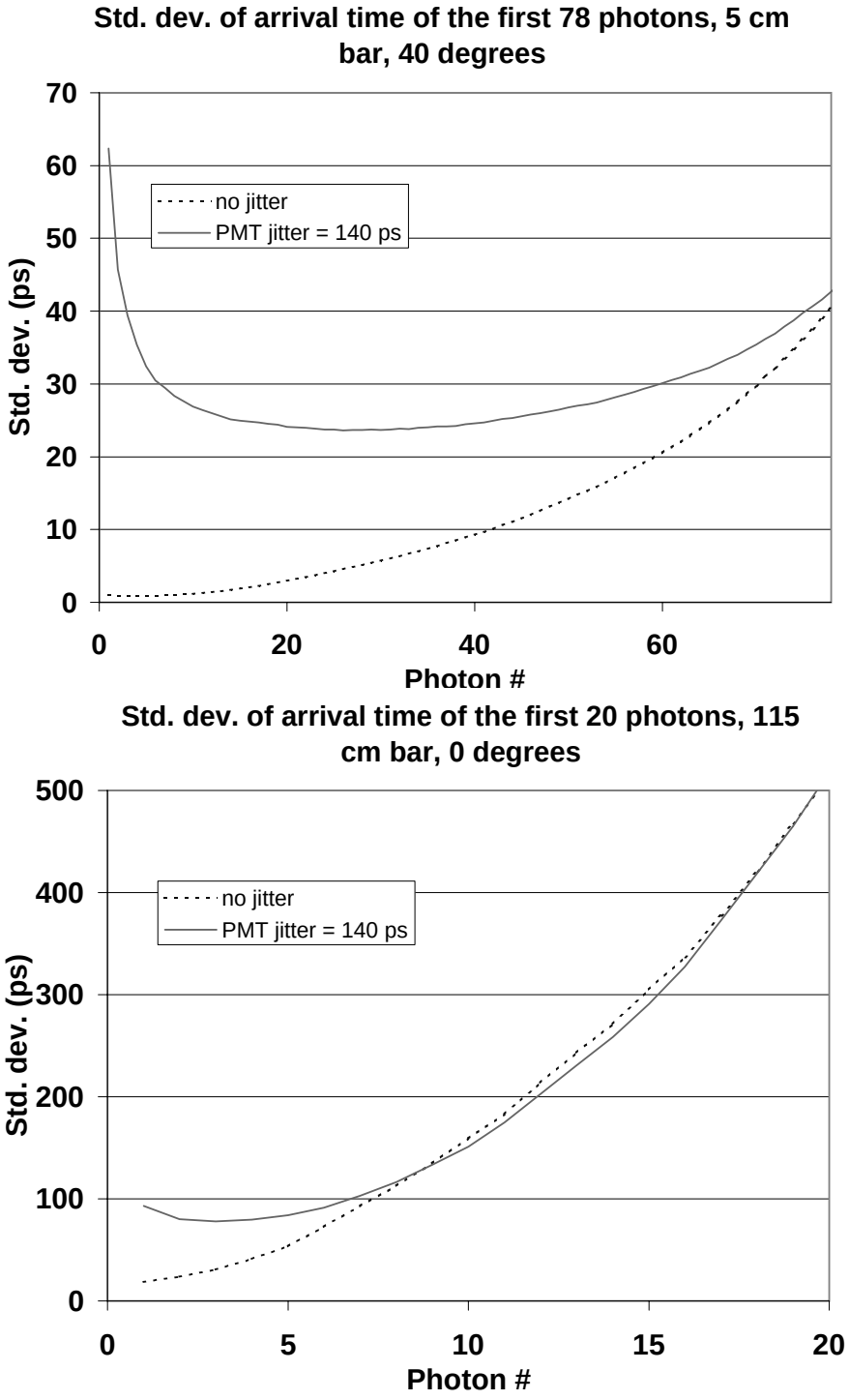

Figure 6: Simulated standard deviations $\sigma_{\mathrm{t,n}}$ of the ordered-photon arrival times for conditions of the experiment of Kichimi *et al.*[3]. First-photon timing is not always the best, once the PMT's transit-time jitter is taken into account.

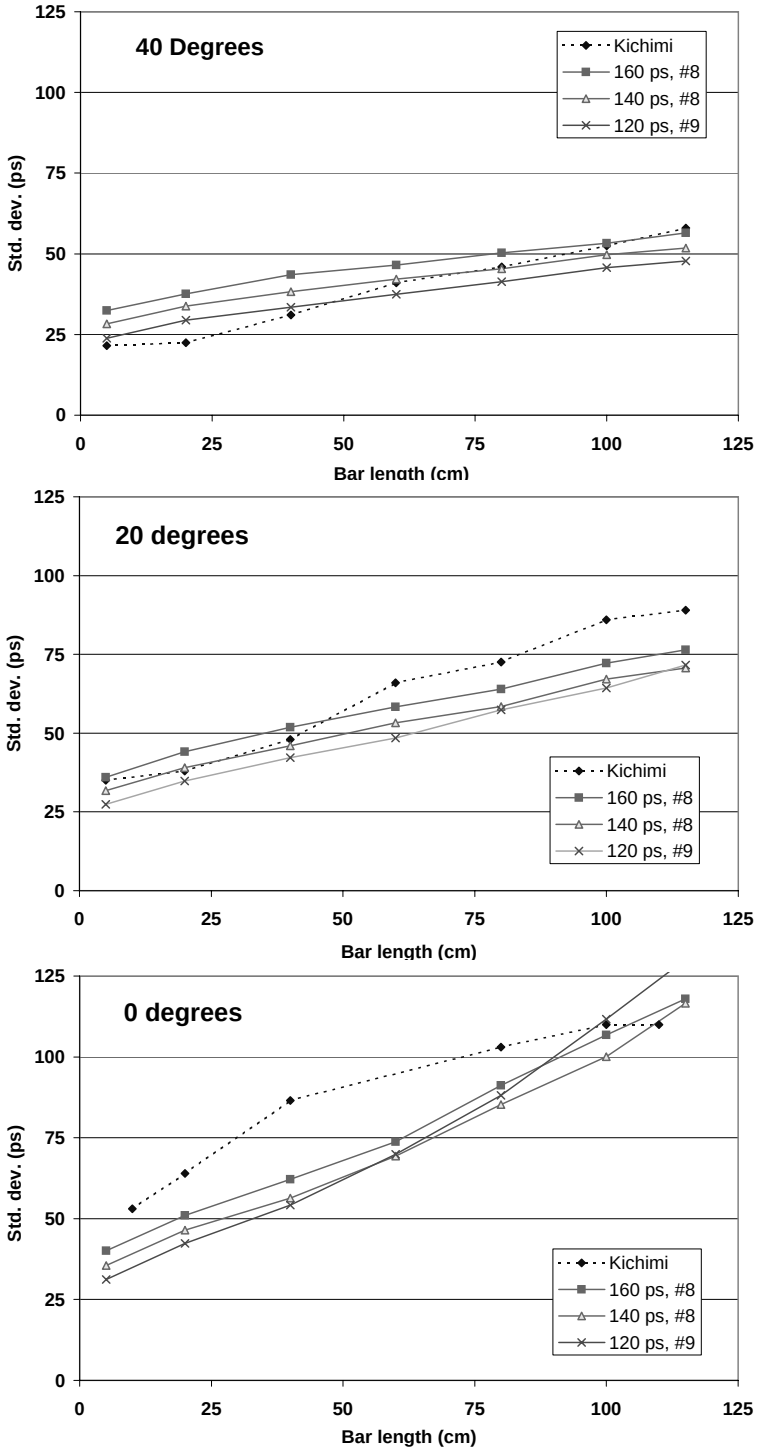

Figure 7: Simulated standard deviation $\sigma_{t,8}$ of the arrival time of the 8th ordered photon for various assumptions as to the PMT transit-time jitter. The results of Kichimi *et al.* [3] are shown for comparison.

relatively good fit to the experimental data by choosing the 8th photon, as shown in Fig. 7 for three values of the PMT transit-time jitter. By choosing a later photon, we could improve the simulated time resolution for a short quartz bar, but this would drastically worsen the time resolution for a long bar. For the 115-cm quartz bar the time jitter seems to increase exponentially with photon number for photons after the 5th. In order to reproduce time resolution as good as $\sigma_t \approx 23$ ps (reported for the 5-cm quartz bar at $\theta_i = 40^\circ$) for photon number 8, we infer that the PMT transit-time jitter $\sigma_{\rm TT}$ was 140 ps rather than 160 ps as quoted by Hamamatsu.

5 Timing of 165-MeV/c Muons with MCP-PMT's

Having calibrated our simulation against experimental data, we can estimate the time resolution for a scenario that would be appropriate for the muon cooling experiment [1].

5.1 The New Scenario

The particles simulated are now 165-MeV/c muons, resulting in a nominal Čerenkov angle $\theta_C = 36^\circ$ in quartz. The critical angle for total internal reflection at the quartz/air boundary is 43°. Therefore, at normal incidence ($\theta_i = 0$) all of the Čerenkov photons would be lost. To avoid this, the quartz bar should be oriented at an angle to the nominal muon trajectory. At $\theta_i = 54^\circ$, for instance, part of the Čerenkov cone would be directed down the quartz bar toward the PMT without any internal reflection, possibly leading to favorable timing characteristics.

To achieve the best time-resolution possible with commercial PMT's, we propose to view the Čerenkov photons with Hamamatsu H3809U microchannel-plate photomultipliers. Hamamatsu reports a transit-time spread of 25-ps FWHM [4] for these devices, which corresponds to $\sigma_{\rm TT} = 10.6$ ps for a Gaussian transit-time distribution. Several recent experiments indicate, however, that the FWHM transit-time jitter is more like 32 ps [8, 9, 10]. In view of this ambiguity, we predict time resolutions for the cases of $\sigma_{\rm TT} = 11$ ps as well as $\sigma_{\rm TT} = 13.5$ ps.

The useful photocathode diameter of the Hamamatsu H3809U is 11 mm. Using quartz bars with a 1×1 cm cross section, the photocathode would cover 89% of the bar's cross-sectional area. We incorporate this in our simulation by disregarding each photon by a random selection with probability 0.11.

The Hamamatsu H3809U is equipped with a quartz window, which has a wider region of transparency than the borosilicate window of the PMT used in the experiments by Kichimi *et al.*The low-wavelength dropoff is now dominated by the wavelength-dependent attenuation in the quartz bar (Fig. 2), and the quantum-efficiency curve of the PMT (Fig. 3). By using ultraviolet-grade quartz bars, we maximize our bandwidth and the number of detected photons per muon.

5.2 Timing Device for the Muon Cooling Experiment

A possible configuration for a timing device is shown in Fig. 8. Since the time jitter increases with bar length, the bars are arranged in two arrays each covering half the beam area. The opening angle between the two halves corresponds to $180^\circ - 2\theta_i$. Increasing θ_i results in better resolution due to more photons and more favorable TIR conditions. However, increasing θ_i increases the path length, and hence the attenuation, of the Čerenkov photons inside the bar.

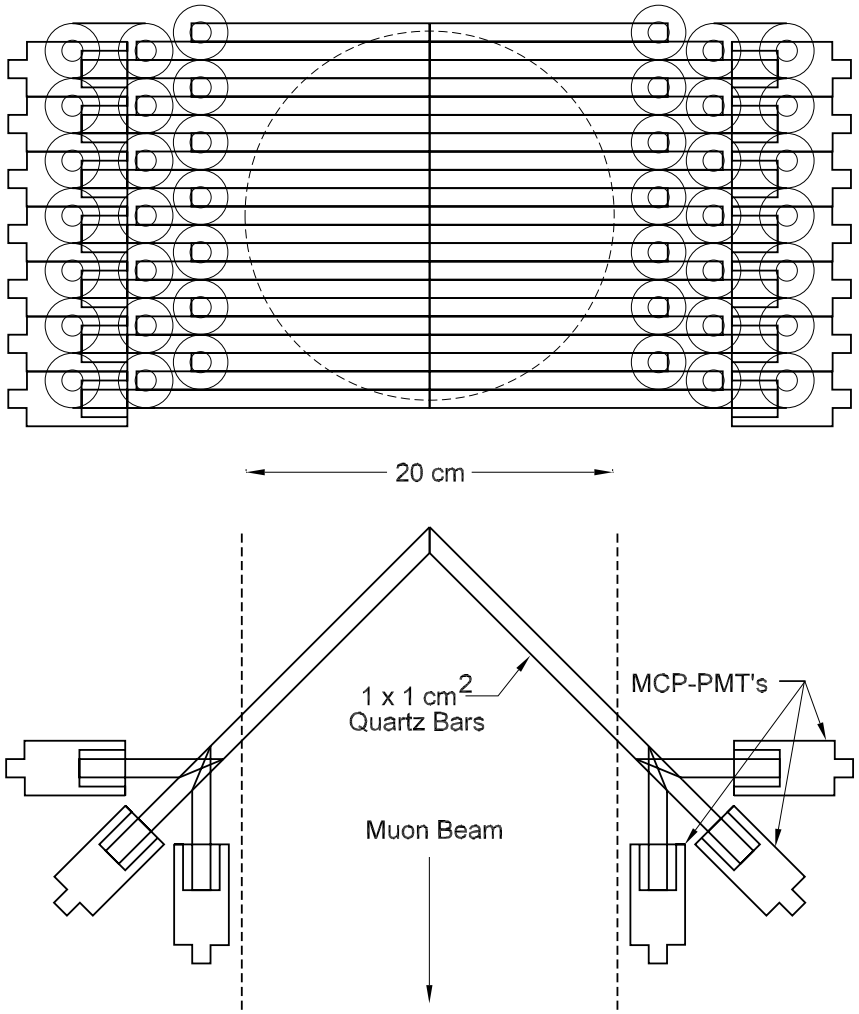

Figure 8: Proposed timing device based on Hamamatsu R3809 MCP-PMT's viewing Čerenkov light from a muon beam of 10-cm radius hitting 1×1 cm^2 quartz bars.

To determine the optimum opening angle, we simulated the time resolution for a range of angles of incidence θ_i with corresponding quartz bar lengths given by $z = r/\cos\theta_i$, where r is the perpendicular distance from the beam axis to the PMT's (in case of straight bars).

Since the nominal beam radius in the detector sections of the cooling experiment is 10 cm, r will need to be at least be 10 cm. In general, r will be greater than this, as needed to array the PMT's so as not to hit one another, as shown in Fig. 8. For our initial simulation we chose $r = 20$ cm, which gives us 10 cm of radial space outside the beam to arrange the photomultipliers.

5.3 Results

The predicted time resolution for the case $r = 20$ cm and various θ_i can be seen in Table 1 assuming $\sigma_{\rm TT} = 13.5$ ps, and Table 2 for $\sigma_{\rm TT} = 11$ ps. The optimum ordered-photon number appears to be $n = 2$, and the optimum angle of incidence θ_i seems to be around 45°, corresponding to an opening angle between the two detector arms of 90°. At this angle, we predict an average of 60 detected photons per event, resulting in a time resolution of $\sigma_{t,2} = 10$ ps.

Fig. 9 shows the time resolutions $\sigma_{t,n}$ of the first 20 ordered photons for $\theta_i = 45^\circ$, $r = 20$ cm and various $\sigma_{\rm TT}$. Comparison of the upper two curves with the lowest curve, which excludes PMT transit-time jitter, indicates that we are in fact approaching the intrinsic time resolution of the device, estimated to be $\sigma_t = 5.6$ ps.

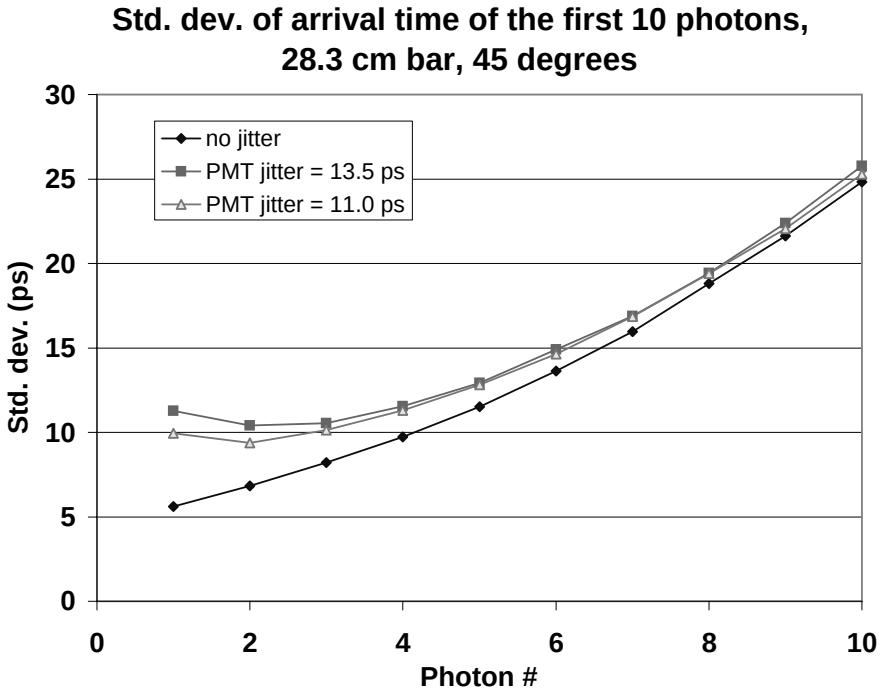

Figure 9: Standard deviation $\sigma_{t,n}$ of arrival time of the first 10 photons for the timing device of Fig. 8 with opening angle 90°, various transit-time jitters, and $r = 20$ cm.

Since the standard deviation of the photon arrival times seem to increase linearly with quartz-bar length (Fig. 7), there is a large potential advantage in reducing r by arranging

Table 1: Predicted time spread of arrival time ($\sigma_{t,n}$) for the first 7 ordered Čerenkov photons from 165-MeV/c muons for various quartz-bar lengths and angles of incidence. The assumed PMT transit-time spread is $\sigma_{\rm TT} = 13.5$ ps.

θ_i	Bar Length	$\sigma_{t,n}$						
(deg)	(cm)	(ps)						
		$n=1$	$n=2$	$n=3$	$n=4$	$n=5$	$n=6$	$n=7$
34	24.1	11.3	**10.6**	11.6	13.4	15.8	19.0	22.4
36	24.7	11.4	**10.6**	11.3	12.6	14.8	17.6	20.8
38	25.4	11.2	**10.4**	11.2	12.7	14.5	17.1	19.9
40	26.1	11.2	**10.3**	10.6	11.6	13.2	15.4	18.2
42	26.9	11.2	**10.3**	10.9	12.0	14.0	16.2	18.5
44	27.8	11.4	**10.3**	10.7	11.5	12.8	14.5	16.9
46	28.8	11.0	**10.1**	10.3	11.1	12.3	14.2	16.3
48	29.9	11.2	**10.2**	10.6	11.4	12.6	13.9	15.8
50	31.1	11.2	**10.1**	10.3	10.9	11.9	13.1	14.7
52	32.5	11.3	**10.2**	10.4	11.1	11.9	13.3	14.8
54	34.0	11.5	**10.2**	10.3	10.7	11.6	12.7	14.1
56	35.8	11.5	**10.3**	10.5	11.0	11.9	12.7	13.9
58	37.7	11.6	**10.3**	10.6	11.0	11.8	12.7	13.7
60	40.0	11.8	**10.7**	**10.7**	11.1	11.8	12.6	13.5
62	42.6	12.1	10.6	**10.5**	10.8	11.4	12.0	12.8
64	45.6	12.1	10.9	**10.7**	11.0	11.4	12.1	12.9

the timing device somewhat differently. For instance, rather than having all quartz bars stacked together in a single array, one could displace neighboring bars along the beam axis so that the PMT's no longer interfere. This would enable the PMT's to be mounted only a few cm outside the beam. Figure 10 shows that as r approaches 10 cm (corresponding to $z = 14.1$ cm on graph), the time resolution approaches 6-7 ps. However, some muons at

Table 2: Predicted time spread of arrival time ($\sigma_{t,n}$) for the first 9 ordered Čerenkov photons from 165-MeV/c muons for various quartz-bar lengths and angles of incidence. The assumed PMT transit-time spread is $\sigma_{\rm TT} = 11.0$ ps.

θ_i	Bar Length	$\sigma_{t,n}$						
(deg)	(cm)	(ps)						
		$n=1$	$n=2$	$n=3$	$n=4$	$n=5$	$n=6$	$n=7$
34	24.1	10.0	**9.5**	10.5	12.5	15.2	18.6	22.2
36	24.7	9.9	**9.4**	10.2	11.8	14.3	17.1	20.6
38	25.4	10.2	**9.7**	10.5	12.0	13.9	16.4	19.5
40	26.1	9.8	**9.2**	9.8	11.1	13.0	15.7	18.8
42	26.9	9.9	**9.1**	10.0	11.2	12.8	15.1	17.6
44	27.8	9.9	**9.2**	9.7	10.9	12.4	14.2	16.8
46	28.8	10.1	**9.3**	9.8	10.8	12.4	14.1	16.3
48	29.9	9.8	**9.3**	9.8	10.7	12.2	13.7	15.5
50	31.1	9.9	**9.2**	9.7	10.5	11.7	13.2	14.7
52	32.5	10.0	**9.5**	9.7	10.5	11.5	12.8	14.5
54	34.0	10.2	**9.5**	9.7	10.6	11.5	12.8	14.1
56	35.8	10.1	**9.4**	9.5	10.3	11.3	12.4	13.7
58	37.7	10.3	**9.4**	9.9	10.5	11.3	12.3	13.3
60	40.0	10.4	**9.6**	9.9	10.5	11.3	12.3	13.3
62	42.6	10.8	**9.9**	10.0	10.5	11.2	12.1	13.0
64	45.6	11.4	**10.3**	10.4	10.6	11.1	11.8	12.6

large angles to the beam might pass through the a sparsely arrayed timing device without hitting any quartz bar.

Note also that timing of muons away from the beam center would be somewhat better than that of muons at beam center which are assumed in the cases above.

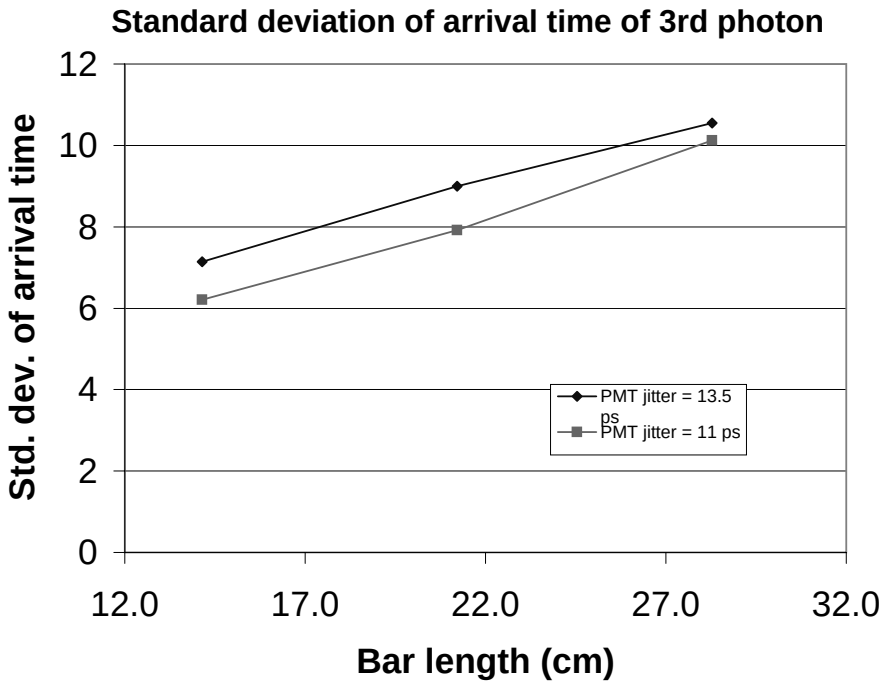

Figure 10: Standard deviation of arrival time $\sigma_{t,3}$ of the 3rd photon for the detector of Fig. 8 with opening angle of 90°, various transit time-jitters, and bar lengths $z = r/\cos(45°)$ for $r = 10$, 15 and 20 cm.

6 Discussion/Conclusion

Our simulation predicts that a device similar to that in Fig. 8 could measure the arrival time of muons over a beam of 10-cm radius with an accuracy of $\sigma_t = 10$ ps. This result is extremely encouraging, and suggests that a beam test be performed to verify it.

In the near future, we will add discussion as to the choice of algorithm for best timing, comparing nth-ordered-photon timing to algorithms that include time averaging. Analytic expressions for many aspects of nth-ordered photon timing will be presented.

7 References

[1] C.M. Ankenbrandt *et al.*, *Ionization Cooling Research and Development Program for a High Luminosity Muon Collider*, (April 15, 1998);
http://www.fnal.gov/projects/muon_collider/cool/proposal/proposal.ps

[2] C. Lu *et al.*, *A Detector Scenario for the Muon Cooling Experiment*, Princeton/$\mu\mu$/97-8 (May 15, 1998);
http://puhep1.princeton.edu/mumu/mumu-97-8.ps

[3] H. Kichimi *et al.*, *The Čerenkov correlated timing detector: beam test results from quartz and acrylic bars*, Nucl. Instr. and Meth. **A371**, 91 (1996).

[4] *Technical Data: Ultrafast MCP-PMT R3809U*, Hamamatsu (Aug. 1992); http://puhep1.princeton.edu/mumu/MCP-1.gif

[5] http://photon.bu.edu/melles/sect-4/sect-4-11.html
http://photon.bu.edu/melles/sect-4/drawing/4-12.jpg

[6] http://www.besoptics.com/html/hereaus-suprasil.html

[7] A.H. Sommer, *Photoemissive Materials* (Wiley, New York, 1968).

[8] B. Gompf *et al.*, *Resolving Sonoluminescence Pulse Width with Time-Correlated Single Photon Counting*, Phys. Rev. Lett. **79**, 1405 (1997).

[9] Robert A. Hiller, Seth J. Putterman, and Keith R. Weninger, *Time-resolved Spectra of Sonoluminescence*, Phys. Rev. Lett. **80**, 1090 (1998).

[10] Michael J. Moran and Daren Sweider, *Measurements of Sonoluminescence Temporal Pulse Shape*, Phys. Rev. Lett. **80**, 4987 (1998).